ARTICLE

Diffusion and Flow Across Nanoporous Polydicyclopentadiene-Based Membranes

William A. Phillip, Mark Amendt, Brandon O'Neill, Liang Chen, Marc A. Hillmyer, and Edward L. Cussler

Department of Chemistry and Department of Chemical Engineering and Materials Science, University of Minnesota, Minneapolis, Minnesota 55455

ABSTRACT We report gas and liquid transport measurements through membranes that have 40% voids made of 14 nm pores. A reactive polylactide–polynorbornenylethylstyrene block polymer is used as a structural template in the polymerization of dicyclopentadiene during the membrane formation process. After the membrane is cast, the pore structure is formed by etching the polylactide component using dilute aqueous base. The pore structure is isotropic; therefore, there is no need for special alignment techniques. Knudsen diffusion experiments and water flow experiments show pores with a tortuosity of 1.81 and a size of 14 nm, a diameter consistent with nitrogen adsorption and small-angle X-ray scattering measurements. These membranes are effective for ultrafiltration, with molecular weight cutoffs (MWCO) consistent with theoretical predictions with no adjustable parameters. These MWCO's can be tuned by changing the size of the constituent blocks in the templating copolymer.

KEYWORDS: block copolymers • nanoporous membranes • filtration • Knudsen diffusion

INTRODUCTION

Block polymers offer a potential route to superior ultrafiltration membranes (1–6). For example, these hybrid macromolecules have been used as membrane casting solution additives in order to impart specific functionality to the membrane surface and/or pore walls (1, 2). The addition of hydrophilic functionality is employed to enhance the membrane's resistance to fouling. Novel membranes have also been prepared by exploiting the self-assembling characteristics of block polymers (3–6). Nanoscopically structured thin films containing hexagonally packed cylinders of one component oriented perpendicularly to the surface of the film have been prepared using neat block polymers (7, 8). When these cylinders are removed by selective etching, the resulting pores are closely packed and are monodisperse (9). Such membranes show potential for ultrafiltration because the monodispersed pores should give high selectivity, and their close packing should allow high fluxes. In addition, flat surfaces can be readily achieved, suggesting that fouling will be reduced (10). However, the cylinders in the self-assembled structure must be oriented perpendicular to the membrane surface for this advantage to be present.

In this research, we avoid the formidable problem of alignment by using a bicontinuous network structure where the "doubly reactive" block polymer polynorbornenylethylstyrene-polylactide is used as a structural template during the metathesis-induced cross-linking of dicyclopentadiene. After subsequent etching of the polylactide component with dilute base, the tough polydicyclopentadiene membrane remaining has an isotropic nanoporous structure (11). Such a membrane has narrowly dispersed pore sizes and so should give high selectivity. Additionally, the membrane's pores are closely packed and so should be capable of high flux.

This work explores the details of the membrane geometry by measuring the diffusion of a variety of gases and flow of water at various values of pH and ionic strength. We demonstrate membrane selectivity through transport studies with a series of polyethylene oxides and a mixture of dextrans. Furthermore, the research shows that the promise of these membranes is real, but it also identifies additional barriers that need to be overcome to realize practical value.

BACKGROUND

The membrane behavior reported below reflects Knudsen diffusion of gases and laminar flow of liquids. In the Knudsen regime (12), the mean free path of the gas molecules is larger than the diameter of the pores. This means that collisions of gas molecules are with the pore walls, not with other gas molecules. A simple model for Knudsen diffusion (12, 13) in a single pore predicts that the diffusion coefficient D_{Kn} is

$$D_{Kn} = \frac{2d}{3}\left(\frac{2k_BT}{\pi\tilde{m}}\right)^{1/2} \quad (1)$$

where d is a characteristic pore dimension, k_B is Boltzmann's constant, T is the temperature, and $\tilde{m}$ is the mass of a diffusing gas molecule. Note that this theory predicts that the diffusion coefficient is independent of pressure but proportional to pore size.

If the diffusing gases were not in the Knudsen regime, intermolecular interactions would dominate the rate of diffusion. In this case the self-diffusion coefficient can be calculated using the kinetic theory of Chapman and Enskog (12). This theory gives a diffusion coefficient, D_{CE}

Received for review October 23, 2008 and accepted January 2, 2009

DOI: 10.1021/am8001428

Published on Web 01/30/2009

$$D_{CE} = \left(\frac{4(2^{1/2})}{3\pi^{3/2}}\right)\frac{(k_B T)^{3/2}}{P\sigma^2 \tilde{m}^{1/2}\Omega} \quad (2)$$

where P is the pressure, σ is the collision diameter, and Ω is a dimensionless function of temperature which is of order 1. Note that, for this type of diffusion, kinetic theory predicts that the diffusion coefficient varies inversely with pressure but is independent of pore size.

Using our experiments, we want to investigate the selectivity of the membranes for different gases. This selectivity should be proportional to the inverse square root of the molecular weight ratio. If modes of transport other than Knudsen diffusion are occurring, such as bulk diffusion, the selectivity would deviate from this predicted ratio. A $(1/\tilde{m})^{1/2}$ term does appear in eq 2, but Ω, the term that accounts for the Leonard-Jones 6-12 potential, causes the ratio of bulk diffusion coefficients to deviate from an inverse square root dependence.

For a porous solid, the effective diffusion coefficient across the film in the Knudsen regime is predicted (13, 14) to follow a modified version of eq 1

$$D_{eff} = \frac{\varepsilon}{\tau}\frac{2d}{3}\left(\frac{2k_B T}{\pi\tilde{m}}\right)^{1/2} \quad (3)$$

where ε is the void fraction and τ is the tortuosity. The void fraction accounts for the experimental measurements being based on the total projected area of the membrane and not on the cross-sectional area of the pores. The tortuosity accounts both for variations in the size and shape of the pore cross-section and for the additional distance required for a molecule to travel relative to the film thickness.

As for the experiments with gases, our measurements of liquid flow center on the calculation of a single transport property, the superficial velocity v

$$v = \frac{\varepsilon}{\tau}\langle v\rangle \quad (4)$$

where $\langle v\rangle$ is the Hagen–Pouiseuille velocity of fluid in a single pore. The Hagen–Pouiseuille relationship (12, 15) gives a velocity of

$$\langle v\rangle = \frac{d^2\Delta P}{32\mu l} \quad (5)$$

where d is the characteristic pore dimension, ΔP is the pressure drop, μ is the liquid viscosity and l is the membrane thickness. This equation does describe liquid flow in nanometer-sized cylindrical pores (16).

We want to use the results of our gas diffusion and liquid flow experiments to further investigate the microstructure of the thin films. As shown in eqs 3 and 5, the effective diffusion coefficient and superficial velocity are functions of ε, τ, and d: three parameters related to the pore structure. The void fraction is readily calculated from the known volume fraction of the etchable component. However, the tortuosity and pore diameter are not well-defined. The effective diffusion coefficient and superficial velocity depend on the pore diameter differently, namely d vs d^2, respectively. Therefore, we can combine our results in order to separate the variables and obtain estimates for d and τ. These estimated values can then be compared to values obtained using independent material characterization techniques. The pore dimension can be inferred from scanning electron microscopy (SEM), from N_2 adsorption/desorption, (13) or from small-angle X-ray scattering (SAXS) experiments (17). Several attempts have been made to calculate tortuosities for known geometries using simulations (18). We will compare our values with these calculations.

We also want to explore the use of these nanoporous membranes as ultrafilters which reject dissolved solutes. To analyze our rejection data, we will use the model of a spherical solute in a cylindrical pore described by λ (19), the ratio of solute diameter to pore diameter. Results like these are described by a sieving coefficient (20)

$$S_a = \frac{c_{1l}}{c_{10}} = \frac{K_c(1-\lambda)^2}{1-(1-K_c(1-\lambda)^2)e^{-[vK_c l/\varepsilon D K_d]}} \quad (6)$$

where c_{1l} and c_{10} are the solute concentrations at the downstream and upstream membrane surface, D is the solute's diffusion coefficient in bulk liquid, and K_c and K_d are tabulated dimensionless factors describing the hinderance of small pores. Note that the dimensionless quantity in brackets is the Peclet number, a measure of the speed of convection relative to the speed of diffusion. We note that the actual sieving coefficient, S_a, is distinct from the observed coefficient, S_o (21). The actual sieving coefficient is calculated using the solute concentration immediately adjacent to the membrane surface, while the observed sieving coefficient replaces this with the bulk upstream solute concentration. While the bulk concentration is more easily obtained in experiments, it can often be lower than the concentration at the membrane surface due to concentration polarization. We will report experiments here without such polarization but recognize that such experiments may not always be possible.

Table 1. Membrane Solutions for Each Sample[a]

sample name	PLA M_n (kg mol^{-1})	amt of P(N-s-S)-PLA (mg)	amt of DCPD (mg)	amt of THF (mL)	amt of catalyst (mg)	f(PLA)
A	32	400	104	2.1	2.9	0.43
B	42	402	109	1.6	2.1	0.47
C	65	402	200	2.0	3.3	0.47

[a] The M_n value of the P(N-s-S) block in each of the examples is 27 kg mol^{-1}.

EXPERIMENTAL SECTION

Membrane Preparation. Thin films of nanoporous polymer were produced using a previously reported method (11). Three samples of polylactide–polynorbornenylethylstyrene (PLA-b-P(N-s-S)), the doubly reactive block polymer that templates the nanopores, are used in this work. All samples had a P(N-s-S) block with a number average molecular weight (M_n) of 27 kg mol^{-1}. In order to observe the effect on pore size, the molecular weight of the etchable PLA block is varied between the samples. The general membrane preparation procedure is as follows: a PLA-b-P(N-s-S) sample is combined with dicyclopentadiene (DCPD) and the second-generation Grubbs metathesis catalyst (22) in the solvent tetrahydrofuran (THF), mixed for about 10 s before being cast onto a glass plate, and allowed to react and partially dry at room temperature for 6 h. The recipes for each membrane sample are given in Table 1.

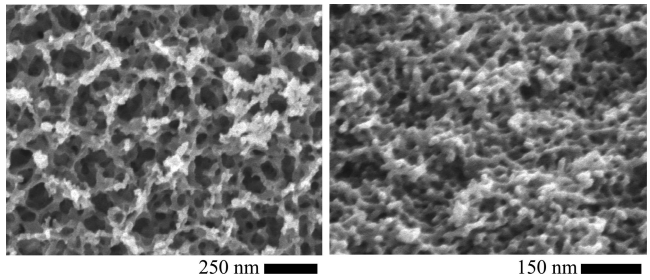

FIGURE 1. SEM image of a typical nanoporous membrane used in this study. The percolating pore structure was templated using a PLA-b-P(N-s-S) polymer. The P(N-s-S) cross-linked the DCPD matrix, and the PLA was etched with a NaOH solution to create the pores.

The optically transparent films (area ca. 100 cm^2 and thickness 100 μm) were then cured at 100 °C for 1 h. After they were cured, the films were removed from the glass plate and exposed to 0.5 M NaOH solution (in 60/40 (v/v) methanol/water) at 70 °C to etch the PLA. After PLA removal, the films were generally treated by an oxygen-reactive ion etch to remove a submicron, nonporous PDCPD "skin" that formed at the surface of the films. The resulting film is a nanoporous composite polyDCPD membrane that can be used for gas diffusion, liquid convection, and ultrafiltration experiments. Typical SEM images of the film's surface (left) and fractured cross section (right) showing the nanoporosity are given in Figure 1. The distribution in pore sizes visible in the image of the film's surface is due to the bicontinuous nature of the material. If we cut across a pore at an angle other than perpendicular, then the pore will appear to be larger than it actually is. The SEM image of the fracture cross-section demonstrates that the pore structure is homogeneous along the length of the membrane.

Gas Diffusion. Thin films approximately 7 mm × 7 mm were cut from larger samples for mounting into the gas diffusion cell. The section was fixed over a 0.3 cm diameter hole in a stainless steel disk, giving an active area of 0.071 cm^2. The section of thin film was held in place using epoxy (DP-460 Off White, 3M, St. Paul, MN) that was applied using a spatula and then allowed to cure overnight at room temperature. The sample was then mounted in the diffusion cell, consisting of two compartments with equal volumes of 15 cm^3 separated by the membrane, as described previously (3). Once the membrane was clamped in the cell, both the donating and receiving solutions were flushed for 90 min with the gas being studied. The receiving solution was then brought to atmospheric pressure, and a 20 psig charge of the diffusing gas was placed in the donating volume. The two compartments were closed, and the data acquisition program was started. Experiments usually lasted about 1 h, and replicate runs were performed after 15 min of additional flushing.

The pressure data were adjusted for small temperature fluctuations using the ideal gas law. The permeability is calculated from

$$\frac{\Delta P_o}{\Delta P} = \exp\left[\frac{D_{eff}\beta t}{l}\right] \qquad \beta = A\left(\frac{1}{V'} + \frac{1}{V''}\right) \tag{7}$$

where A is the membrane area, t is the time, V' and V'' the receiving and donating compartment volumes, respectively, and ΔP_o and ΔP are the pressure differences between the donating and receiving compartments initially and at time t. The data are plotted as $\ln(\Delta P_o/\Delta P)$ vs t/l, and D_{eff} is determined from the slope.

Liquid Convection. Liquid convection experiments were performed using a stirred filtration cell (Amicon 8010, Millipore Co., Billerica, MA) that has an active area of 4.1 cm^2. Circular disks 2.5 cm in diameter were cut from the cast sheet to fit into the stirred cell and sealed with a silicone O-ring. The pressure difference that drives convection was applied using N_2 gas (UHP N_2, Airgas, Radnor Township, PA). Prior to beginning flux measurements, the membrane was prewet using isopropyl alcohol for 30 min and flushed with pure water for 45 min to remove the alcohol. Besides wetting of the membrane, no other preconditioning was required; specifically, no period of compaction was required. The observed flux of pure water through the membrane was not a function of time, indicating that little to no compaction occurred when a pressure drop was applied across the membrane. This is to be expected, given the rigidity of our membrane and the relatively low pressure drop applied. Once the membrane had been wet and flushed, the stir bar was turned off and the pressure set to the desired value. The permeating water was collected in a glass vial and its mass measured (Mettler-Toledo, Inc., Columbus, OH) every 5 min for 1 h. Flow rate measurements were performed three times at each pressure drop to check reproducibility.

Table 2. Molecular Eeight and Characteristic Size of PEO Solutes

	R_H (nm)	
PEO sample M_n (kg mol^{-1})	$D_t(23)$	$\eta(24)$
0.75	0.6	0.8
3.40	1.5	1.8
8.90	2.6	3.2
14.0	3.4	4.0
23.5	4.5	5.4
35.0	5.7	6.8
59.0	7.8	9.0

Ultrafiltration. Two types of feed solutions were used to challenge the nanoporous membranes. The first type was a solution of a single polyethylene oxide (PEO) sample (Polymer Source Inc., Montreal, Quebec, Canada) with a narrow molecular weight distribution dissolved at a concentration of 1.5 g L^{-1}. Single-solute experiments were performed using seven different PEO molecular weights (0.8, 3.0, 9.0, 14.0 23.0, 34.5, and 59.0 kg mol^{-1}), selected because the molecules have hydrodynamic radii in the size range of the pores (Table 2). The hydrodynamic radii were calculated using published data which show how the tracer diffusion coefficients (23) and intrinsic viscosities (24) vary with polymer molecular weight. The Stokes−Einstein equation (eq 8) was used to calculate the PEO hydrodynamic radius from experimental tracer diffusion data (23)

$$D_t = \frac{k_B T}{6\pi\mu R_H} \tag{8}$$

where D_t is the diffusion coefficient of an individual polymer chain, k_B is Boltzmann's constant, T is temperature, μ is the liquid viscosity, and R_H is the hydrodynamic radius. The hydrodynamic radius of the PEO molecules can also be estimated using intrinsic viscosity data for the aqueous polymer solutions (24) (eq 9)

$$\eta = \frac{10\pi N_A R_H^{\,3}}{3M_n} \tag{9}$$

where η is the intrinsic viscosity of the polymer solution, N_A is Avogadro's number, and M_n is the number-average molecular weight of the polymer sample.

The concentrations of PEO in the feed and permeate solutions were determined using total organic carbon (Sievers 900 por-

table TOC analyzer, GE Analytical Instruments, Boulder, CO). Because the detection range of the TOC was 0−20 ppm, the collected feed and permeate samples were diluted 100-fold with water. Calibration solutions for each PEO molecular weight were made at 1, 5, 10, 15, and 20 ppm because there was some concern about the higher molecular weight samples not being fully oxidized.

The second type of feed solution used was a mixed solute solution consisting of polydisperse dextran fractions in 18 MΩ water. The concentration of the individual dextran fractions were selected to match the guidelines set out by ASTM 1343: Standard Test Method for Molecular Weight Cut-Off Evaluation of Flat Sheet Ultrafiltration Membranes (25). These concentrations were analyzed using size exclusion chromatography (SEC) in a manner consistent with ASTM 1343. For both types of feed solutions, sieving curves were calculated from the ratio of the concentration in the filtrate to that of the feed solution.

Ultrafiltration experiments were performed with the same membrane preparation and wetting procedures in the same Amicon 8010 stirred cell system as for the liquid convection experiments. Once the membrane was in place, wetted, and flushed, the pure water flux was checked for 1 h at a pressure drop of 13 psig to verify the sample performed in a manner consistent with the membranes used for liquid convection experiments. At this point, the stirred cell was filled with feed solution and the pressure drop returned to 13 psig. The system was run for 1 h to flush the tubing running from the cell to the collection vial, thus avoiding artificial dilution of the collected permeate sample. After flushing, a clean glass vial was used to collect 1 mL of permeate, which was analyzed using either TOC or SEC, depending on the solute type. The system was then rinsed with water and flushed for 1 h with 18 mΩ water. During this time, the flux was remeasured at a pressure drop of 13 psig to make sure no changes had occurred in the membrane. If the water flow rate was similar to that observed before the membrane was challenged, the next solution was put into the cell and the process repeated. In this way we were able to move sequentially through the seven PEO solutions or repeat dextran experiments to check reproducibility.

RESULTS

This research included three different groups of experiments: gas diffusion, liquid convection, and ultrafiltration. The gas diffusion and liquid convection experiments elucidate transport properties of the self-assembled, etched membrane pores, while the ultrafiltration studies begin to explore whether these structures have practical applications. The following paragraphs provide a discussion of the three groups.

Gas Diffusion. These studies measured the pressure difference across the membrane as a function of time for thin films made from polymer sample B. The results, shown in Figure 2, vary as predicted by eq 7. The slope of the curves was used to calculate the effective diffusion coefficient for each gas.

These effective diffusion coefficients, which are reported in Table 3, are reproducible, varying less than ±3% for duplicate experiments with the same membrane or for repeated experiments with different membranes.

The experimental diffusion coefficients can be compared with coefficients calculated using the Knudsen and Chapman-Enskog theories. Except for ammonia, the experimentally measured coefficients are within 10% of those calculated using eq 3. The use of eq 3 relies on the assumption of

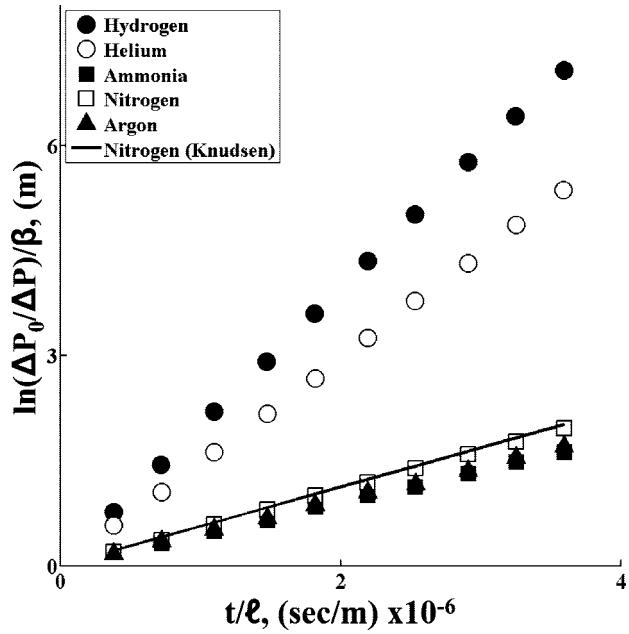

FIGURE 2. Gases diffusing across the membrane by a Knudsen mechanism. The slope of the experimental data is proportional to the gas permeability. Knudsen theory, shown for N_2 as a solid line, predicts a $(1/\bar{m})^{1/2}$ dependence.

Table 3. Summary of Gas Diffusion Data[a]

solute	D_{eff}	D_{eff}/ε^b	D_{Kn}/τ^c	$D_{C\text{-}E}$	$\alpha_{exptl}{}^d$	$\alpha_{Kn}{}^d$	$\alpha_{C\text{-}E}{}^d$
H_2	0.0184	0.0391	0.0464	0.9474	0.84	0.71	1.18
He	0.0154	0.0328	0.0328	1.1184	1.00	1.00	1.00
NH_3	0.0043	0.0091	0.0159	0.1299	3.58	2.06	8.61
N_2	0.0055	0.0117	0.0124	0.1350	2.80	2.66	8.28
Ar	0.0047	0.0100	0.0104	0.1219	3.27	3.15	9.17

[a] All diffusion coefficients are reported with units of cm^2/s. [b] Assuming $\varepsilon = 0.47$. [c] Assuming d = 14.2 nm and $\tau = 1.81$. [d] All selectivities are defined as $\alpha_i \equiv D_{He}/D_i$.

a pore diameter and tortuosity. Here we assumed $d = 14.2$ nm and $\tau = 1.81$. These choices are explained below. Table 3 also presents the selectivities for the gases relative to helium diffusion. Helium was chosen as the reference gas because it was not expected to interact with the solid membrane (26). The experimental selectivities for all gases except ammonia are within an average of 5% of those predicted, demonstrating they have a molecular weight dependence consistent with Knudsen diffusion, i.e. $(1/\bar{m})^{1/2}$. These results show conclusively that transport through the pores occurs by a Knudsen mechanism, which is expected because the mean free paths of these gases are about 10 times larger than the pore diameter (9). The results also indicate that the membranes have nanoscopic pores which span the entire membrane thickness, as transport through macroscopic defects would occur by mechanisms other than Knudsen diffusion.

The somewhat lower values observed for Knudsen diffusion of ammonia are probably a result of an interaction of ammonia with groups on the pore walls left after etching. These interactions are not strong enough to cause ammonia to adsorb onto the pore wall and in turn to reduce the effective pore diameter. Experimental evidence for this can

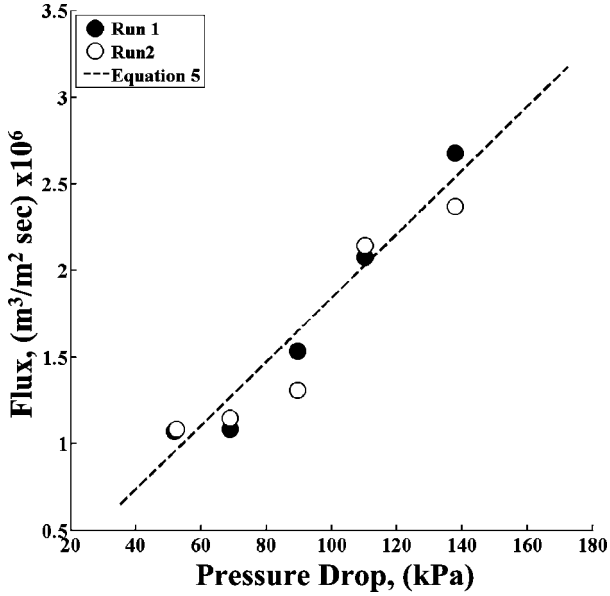

FIGURE 3. Proportionality of water flux to pressure drop. Experimentally observed fluxes for polymer sample B are compared to values from eq 5.

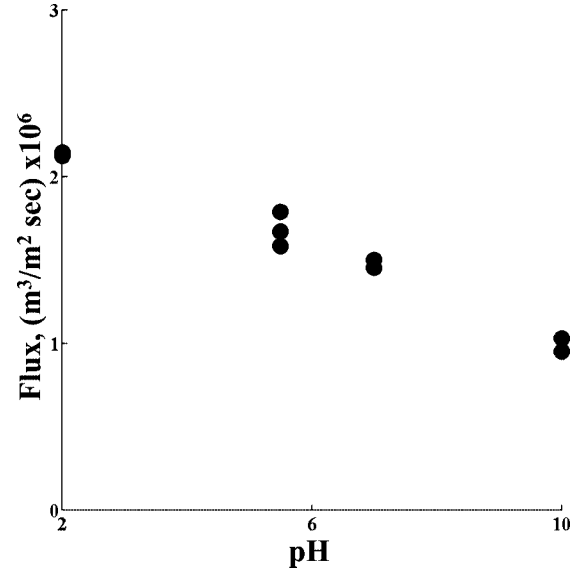

FIGURE 4. Water flux as a function of pH. The flux is shown to be a function of pH at $I = 10^{-3}$ M. The reason for the decrease in flux with increasing pH is not known but may be due to acid groups left in the pore after etching.

be found in the helium diffusion coefficient measured in the presence of an ammonia atmosphere. In the Knudsen regime, diffusing molecules do not collide with each other; therefore, there is no interaction between the ammonia and helium molecules that would affect the measured helium coefficient. However, if ammonia did adsorb onto the pore wall, the effective pore diameter would be decreased, causing a decrease in the measured helium coefficient. Measurements of helium transport in the presence of ammonia do not show such a decline in the helium diffusion coefficient (i.e., the mixed-gas and single-gas values are the same), implying that ammonia is not adsorbing onto the pore walls. The interactions between ammonia and groups on the pore wall invalidate a key assumption of our simple Knudsen model of diffusion, that the collisions between the diffusing solute and pore wall are elastic; more accurate theories of Knudsen diffusion include such features as a sticking coefficient to correct for nonelastic collisions.

Liquid Convection. The flux, in $m^3/(m^2\ s)$, is plotted in Figure 3 vs the pressure drop, in kPa. The linear relation expected from eq 5 is observed. The fluxes are small, around 1×10^{-6} $m^3/(m^2\ s)$ (4 gal/(ft^2 day)) at a pressure drop of 30 kPa. However, if the membrane thicknesses were decreased from 100 μm to 0.5 μm and the pressure drop was increased to 200 kPa, the flux would be predicted to be 2.8×10^{-3} $m^3/(m^2\ s)$ (5600 gal/(ft^2 day)).

If this flux could be achieved, it would be competitive with typical fluxes observed through membranes made by phase inversion. These fluxes are found to range from 3.0×10^{-5} to 4.0×10^{-4} $m^3/(m^2\ s)$. These experiments do not show these high fluxes, though they do suggest the potential of these membranes. Hexagonally packed right cylinders could give a still higher flux, but they are difficult to align. Because the bicontinuous structure used here is isotropic, it requires no special alignment. The price paid is the lower flux and the less well-defined pore structure.

This convective flux is independent of ionic strength over a range of 10^{-3} to 10^{-1} mol/L of NaCl at a pH of 5.5. However, the convective flux is a function of pH, as shown by the data in Figure 4.

Because the membranes are stored in water exposed to room air, their initial pH is 5.5; it was raised or lowered by adding sodium hydroxide or hydrochloric acid. The 60% decrease in flux as the pH changes from 2 to 12 suggests an effective 3 nm decrease in pore size. This can be rationalized as a chemical reaction producing hydrophilic groups within the pore, which then extend further into the center of the pore, reducing its effective diameter. However, we have no independent experimental support, and this does not explain the near-linear variation with pH observed.

A hysteresis was observed when the pH of the permeating solution was changed. The data in Figure 4 represent the steady-state flow rates at a particular pH. After the pH of the permeating solution was changed, there was a period of time over which the steady-state value would slowly be approached. The observed effect occurred for both increases and decreases in pH, with the variation depending on the direction of the pH change. For example, after an experiment at pH 2, flow rates measured at pH 5.5 would be higher for about 2 h. Over that time, the flow rate slowly decayed to the new steady value, while after an experiment at pH 10 the measured flow rates would be lower. This effect was completely reversible: given enough time, flow rates would return to the original steady-state value.

The predictions of Knudsen diffusion and liquid convection do rest on the assumption of a pore diameter and membrane tortuosity. The pore diameter and tortuosity were inferred from experiments by using the measured diffusion coefficient for helium, the hydraulic permeability of water at pH 5.5, and eqs 3−5. This method gave $d = 14.2$ nm and $\tau = 1.81$. These values are compared with other measurements of the pore diameter and tortuosity in Table

Table 4. Comparison of Pore Diameter and Membrane Tortuosity

characterization technique	d (nm)	τ
gas diffusion/liquid flow	14.2	1.81
BET[a]	15.1	
SAXS C[b]	22.3	
SAXS L	11.6	
BJH[c]	16.0−23.0	
SEM	20.0	
theory[d]		1.56

[a] The method used to calculate pore diameter is described in ref 13. [b] The domain spacing was calculated according to ref 17. SAXS C and SAXS L refer to assuming a cylindrical and lamellar morphology, respectively. [c] The Barrett−Joyner−Halenda method is described in ref 27. [d] The tortuosity was taken from simulations in ref 18.

4. In ref 8 we estimated a tortuosity of 2.29 for a similar membrane using only gas diffusion experiments. Here we have assumed the tortuosities for gas diffusion and liquid flows are the same and by doing so are able to use complementary techniques to estimate a tortuosity of 1.81. We are more confident in this value, given its agreement with supportive computational work (18).

The size from diffusion and flow is consistent with values from BET and SAXS, with a level of agreement comparable to that observed earlier for cylindrical pores (3). The values inferred from diffusion and flow are expected to be somewhat less than those measured by other methods, because diffusion implicitly reflects the resistances of pore diameters in series and thus implies a harmonic average of pore diameters. The average size should be smaller than those from methods which average pore sizes differently, as the BJH (Barrett−Joyner−Halenda) analysis does (25). However, the detailed relation between these values is not known because the exact pore geometry is not known.

Ultrafiltration. Finally, we consider the flow of solutions containing macromolecular species across these membranes. Because the dissolved solute's sizes are on the same order of magnitude as the membrane pore size, the solute should be at least partially retained. The membrane's ability to perform such a separation is described by the sieving coefficient S_a, defined as the concentration in the permeate c_{1l} divided by that at the upstream membrane surface c_{10} (eq 6). In practical studies, the concentration at the membrane surface is replaced by the bulk upstream concentration, c_F. The bulk value is often lower than c_{10} due to concentration polarization, where the ultrafiltration itself causes higher solute concentrations at the upstream membrane surface than in the bulk solution. This higher surface concentration in turn reduces the flux (28). This effect is illustrated by the ultrafiltration of a 2% solution of a 35 kD PEO, shown as circles in Figure 5.

The flux drops off as the pressure drop increases. This drop is absent in the ultrafiltration of pure water, shown as filled circles; it is also absent when the upstream solution is rapidly stirred, shown by squares. By always carrying out ultrafiltration experiments with rapid stirring, we avoid this

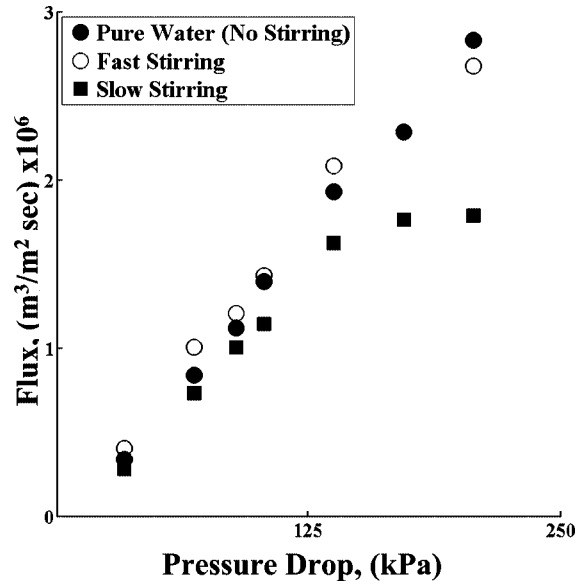

FIGURE 5. Flux of a 2 wt % PEO solution as a function of the stirring rate. Rejected solutes accumulate at the pore wall, causing a decrease in the observed flux. Rapid stirring allows for rapid mass transport of these solutes back to the bulk solution and prevents a decrease in flux.

complexity and measure the sieving coefficients of the membrane directly.

That concentration polarization is negligible is supported by comparing the mass transfer coefficient of solute in the bulk solution, k, to the flux of the permeate, v, across the membrane. The ratio of these values determines how closely the experimentally observed sieving coefficient reflects the membrane's actual sieving coefficient:

$$S_a = \frac{S_0}{(1 - S_0)\exp(v/k) + S_0} \qquad (10)$$

When v/k is small (i.e., concentration polarization is small), S_a and S_0 are about equal. When v/k increases, the concentration polarization does as well, and the observed sieving coefficient is no longer representative of the actual sieving coefficient. Using the correlation given by Zeman and Zydney for a stirred cell geometry at a stirring speed of 400 rpm, we calculate a mass transfer coefficient of 1.1×10^{-5} m/s (29). This mass transfer coefficient and the filtrate flux at 80 kPa give a value for v/k of 0.09. At this flux and stirring speed the system is not highly polarized and our experiments reflect the actual sieving coefficient of the membrane.

These ultrafiltration experiments are summarized for a series of PEO solutes in Figure 6.

The molecular weight of each solute is given next to each data point. The figure plots the percent rejected ($(1 - S_a) \times 100$) vs the solute diameter (i.e., 2 times the hydrodynamic radius) divided by the pore diameter, λ. The solute diameters are estimated as a function of molecular weight from tracer diffusion and intrinsic viscosity measurements given in the literature (23, 24). The pore diameter is taken as a constant 14.2 nm, determined as described above by gas diffusion and liquid flow. This diameter is consistent with the flows in Figure 5 and the diffusion data in Table 3. As expected, the rejection of the 1 kD sample is small, around 4%; it

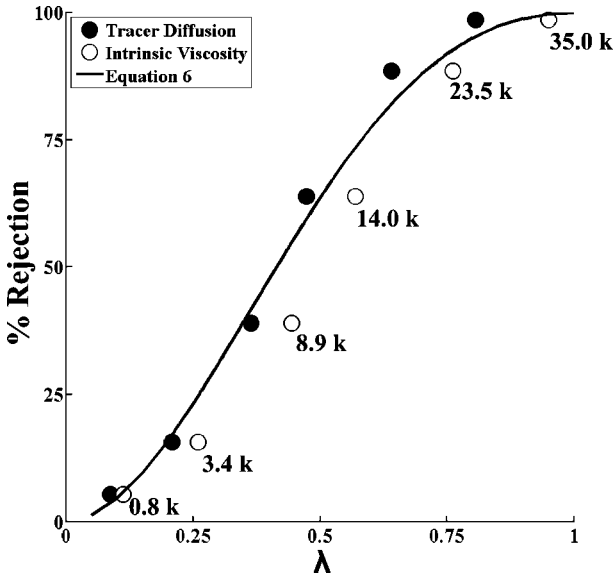

FIGURE 6. PDCPD membrane rejects PEO solutes as expected. Single-solute PEO solutions were used to challenge a PDCPD membrane made using polymer sample B. The resulting rejection curve is compared with the predicted curve using the hindrance coefficients of Brenner (19) for a 14.2 nm pore. The filled circles and open circles are for PEO hydrodynamic radii calculated from tracer diffusion coefficient (23) and intrinsic viscosity (24) data, respectively.

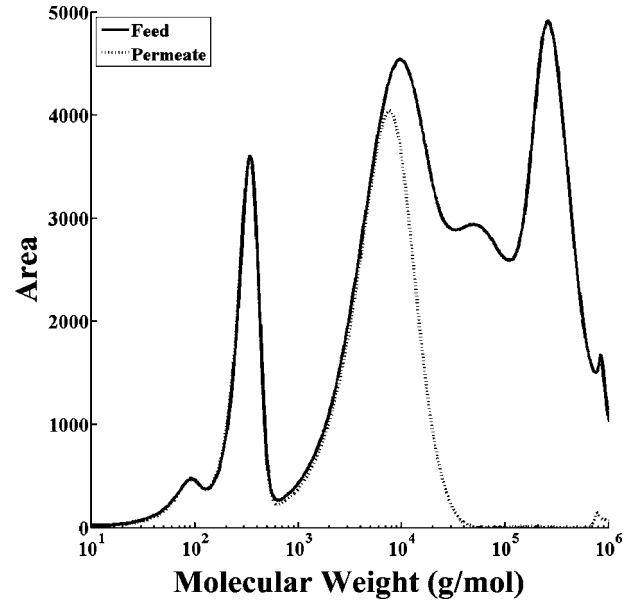

FIGURE 7. Typical SEC data used to calculate the rejection curve for dextran solutions. The mass concentration of dextran in solution is proportional to peak area. The percent rejection is calculated from (1 − (permeate area)/(feed area)) × 100.

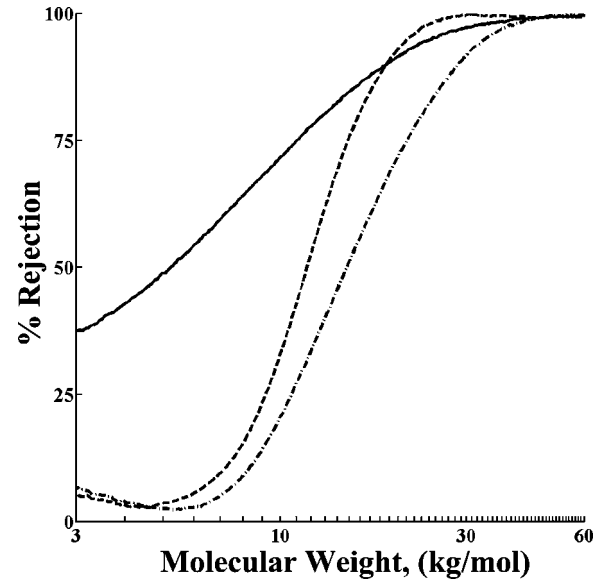

FIGURE 8. PDCPD membranes show a sharper MWCO than a membrane made by phase inversion, shown as the solid line. The dashed and dash-dotted lines are rejection curves for the membranes developed in this work from polymer samples A and C, respectively. By tailoring the molecular weight of the etchable block, the pore size can be modified.

increases with solute molecular weight until the rejection of the 35 kD sample is near complete, over 98%.

The curve shown in Figure 6 is not a best fit of the data but a prediction without adjustable parameters based on eq 6. This prediction depends on the membrane's thickness and void fraction, on the fluid's velocity, on the solute's diffusion coefficient, and on the ratio of solute diameter to pore diameter λ: that is, on the values on the abscissa of Figure 6. From values of λ, we find the parameters K_c and K_d using the equations developed by Bungay and Brenner (19) and then can calculate the curve in Figure 6. The agreement of this curve with the experimental results implies that the membrane pores are nearly monodisperse and reproducible across membranes made from the same polymer sample.

Finally, we made a series of experiments with a mixed feed of dextrans. These experiments imitate quality control studies carried out industrially. In experiments like these, all solutes are fed simultaneously, and the flux of each out of the membrane is determined using SEC equipped with a differential refractometer detector. A sample of the output from the differential refractometer is presented in Figure 7. The ratio of the appropriate peak areas is used to calculate the rejection curves shown in Figure 8.

Using this method, two types of membranes were tested our nanoporous PDCPD membranes and commercial membranes made by phase inversion. Two PDCPD membranes were used, one with a 32 kDa etchable PLA block and the other with a 65 kDa block. This change was made to observe the influence of the PLA molecular weight on the pore dimension. The commercial membrane made by phase inversion is still under development, and details regarding specific characteristics were not given. The scientist who assisted with these experiments selected this membrane because it has a MWCO similar to that of our PDCPD materials. We recognize that this membrane could have a particularly poor rejection curve but doubt this is the case, because it is frequently selected by the manufacturer to test the accuracy of their detection equipment. Experiments with both our nanoporous PDCPD membranes and commercial membranes made by phase inversion were run at a constant pressure drop of 13 psig.

Ideally, we would like these curves to be step functions with no rejection until a critical molecular weight and then

complete rejection above this critical weight. However, this is inconsistent with the underlying theory for Figure 6, where the rejection is gentler because of altered free volume and drag of the solute within the pores. Even though step functions are not possible, the results in Figure 8 are encouraging. The data for our two membranes based on etched, self-assembled, block polymer based membranes show a rejection sharper than those of a commercial ultrafiltration membrane. Moreover, the data for a membrane with a 32 kD PLA block reassuringly show a cutoff at lower molecular weight for a 65 kD PLA block. This suggests that block polymer membrane properties can be further tuned to perform a specific desired separation.

DISCUSSION

The results of our experiments are encouraging. Block copolymer derived nanoporous materials demonstrate some of their potential as an alternative route to ultrafiltration membranes. The MWCO experiments with a mixed dextrans feed show that our films provide a more precise cutoff than ultrafiltration membranes made by phase inversion. These experiments also show that control over the etchable block molecular weight provides the option for finer control over the cutoff location. The gas diffusion, liquid flow, and PEO MWCO experiments all agree with existing theories, and the pore diameter implied by these theories, 14.2 nm, is corroborated by BET and SAXS measurements. These results suggest pursuing further research efforts in order to overcome the obstacles which stand in the way of making ultrafiltration membrane made from block copolymers viable industrial alternatives to current technologies.

To anticipate these alternatives, we remember that ultrafiltration membranes are judged by three criteria: selectivity, flux, and resistance to fouling. The results in Figures 6 and 8 show superior selectivity which can be predicted on the basis of existing theories for cylindrical pores. The fluxes reported in Figures 3 and 4 will be over 10 times faster than those currently used if the membrane thickness can be reduced.

However, these positive results should be tempered by concerns with membrane thickness and pore diameter. At present, these membranes, cast without a support, have a thickness of 100 μm. Such thick membranes result in low fluxes, because the flux is normally inversely proportional to the membrane thickness. Casting membranes which are around 0.5 μm on a nonwoven support is obviously a high priority. Casting membranes which are dramatically thinner than 0.5 μm is less important, because the resistance to flow of the support becomes dominant (28−30). While the membranes studied here have not yet been cast on either flat sheet or hollow fiber supports, several techniques exist for casting a thin selective layer onto a support layer (28). We are confident these methods can be tailored to the constraints our system presents.

The membranes studied here are based on self-assembled bicontinuous structures of a polylactide phase and a polydicyclopentadiene-based phase. When these structures are etched with dilute base, a porous membrane consisting of predominantly polydicyclopentadiene remains. This porous structure is isotropic, so that it requires no alignment to be permeable. The pores fill about 40% of the membrane volume so that the flux is potentially high. However, the porous structure is periodic, so that the pore diameter changes from a small value to a larger one and then back to a smaller one.

Such a structure means that the definition of a pore diameter is ambiguous. Diameters estimated from micrographs will represent only the surface, and diameters found from SAXS will be arithmetic averages of size. Diameters from surface area (i.e., from BET measurements) should be best for convective measurements because fluid drag is also proportional to surface area. These expectations seem supported by experiment.

The superior selectivity and faster fluxes of these easily fabricated membranes may be lost if the membranes foul easily. There is some reason to expect that they will: their internal structure probably does contain some double-conical structures which should plug quite easily. At the same time, the overall surface of the membranes appears on a micrometer scale to be much smoother than that of existing ultrafiltration membranes (10). Therefore, it is critical to experimentally probe the fouling of these membranes and experiments are underway.

Acknowledgment. This work was largely supported by the U.S. Air Force Office of Scientific Research (Grant No. F49620-01-1-0333) and the U.S. Department of Energy (Grant No. 5-35908). This work was supported partially by the MRSEC Program of the National Science Foundation under Award No. DMR-0819885. We are grateful to Trent Biniek and Andrew Back, GE Osmonics, for help in the ultrafiltration measurements.

REFERENCES AND NOTES

(1) Asatekin, A.; Kang, S.; Elimelech, M.; Mayes, A. M. *J. Membr. Sci.* **2007**, *298*, 136–146.
(2) Hancock, L. F. *J. Appl. Polym. Sci.* **1997**, *66*, 1353–1358.
(3) Phillip, W. A.; Rzayev, J.; Hillmyer, M. A.; Cussler, E. L. *J. Membr. Sci.* **2006**, *286*, 144–152.
(4) Yang, S. Y.; Ryu, I.; Kim, H. Y.; Kim, J. K.; Jang, S. K.; Russell, T. P. *Adv. Mater. (Weinheim, Ger.)* **2006**, *18*, 709–712.
(5) Yang, S. Y.; Park, J.; Yoon, J.; Ree, M.; Jang, S. K.; Kim, J. K. *Adv. Funct. Mater.* **2008**, *18*, 1371–1377.
(6) Peinemann, K. V.; Abetz, V.; Simon, P. F. W. *Nat. Mater.* **2007**, *6*, 992–996.
(7) Bates, F. S.; Fredrickson, G. H. *Annu. Rev. Phys. Chem.* **1990**, *41*, 525–557.
(8) Bates, F. S. *Science (Washington, D.C., U.S.)* **1991**, *251*, 898–905.
(9) Olayo-Valles, R.; Guo, S.; Lund, M. S.; Leighton, C.; Hillmyer, M. A. *Macromolecules* **2005**, *38*, 10101–10108.
(10) Zhu, X.; Elimelech, M. *Environ. Sci. Technol.* **1997**, *31*, 3654–3662.
(11) Chen, L.; Phillip, W. A.; Cussler, E. L.; Hillmyer, M. A. *J. Am. Chem. Soc.* **2007**, *129*, 13786–13787.
(12) Cussler, E. L. In *Diffusion, Mass Transfer in Fluid Systems*; Cambridge University Press: New York, 1997; p 580.
(13) Huizenga, D. G.; Smith, D. M. *AIChE J.* **1986**, *32*, 1–6.
(14) Dullien, F. A. L. In *Porous Media: Fluid Transport and Pore Structure*; Academic Press: San Diego, CA, 1992; p 574.
(15) Bird, R. B.; Stewart, W. E.; Lightfoot, E. N. In *Transport Phenomena*; Wiley: New York, 2002; p 895.
(16) Anderson, J. L.; Quinn, J. A. *J. Chem. Soc., Faraday Trans. 1* **1972**, *68*, 744–748.
(17) Teubner, M.; Strey, R. *J. Chem. Phys.* **1987**, *87*, 3195–3200.

(18) Tassopoulos, M.; Rosner, D. E. *Chem. Eng. Sci.* **1992**, *47*, 421–443.
(19) Bungay, P. M.; Brenner, H. *Int. J. Multiphase Flow* **1973**, *1*, 25.
(20) Deen, W. M. *AIChE J.* **1987**, *33*, 1409–1425.
(21) Mehta, A.; Zydney, A. L. *J. Membr. Sci.* **2005**, *249*, 245–249.
(22) Scholl, M.; Ding, S.; Lee, C. W.; Grubbs, R. H. *Org. Lett.* **1999**, *1*, 953–956.
(23) Faraone, A.; Magazu, S.; Maisano, G.; Migliardo, P.; Tettamanti, E.; Villari, V. *J. Chem. Phys.* **1999**, *110*, 1801–1806.
(24) Meireles, M.; Bessieres, A.; Rogissart, I.; Aimar, P.; Sanchez, V. *J. Membr. Sci.* **1991**, *103*, 105–115.
(25) Standard Test Method for Molecular Weight Cutoff Evaluation of Flat Sheet Ultrafiltration Membranes; ASTM-ASTM International, 2001; ASTM E 1343-90 (reapproved 2001).
(26) Yang, R. T. In *Gas Separation by Adsorption Processes*; Imperial College Press: Singapore, 1997; Series on Chemical Engineering, Vol. 1, p 352 (distributed by World Scientific, London, River Edge, NJ).
(27) Barrett, E. P.; Joyner, L. G.; Halenda, P. P. *J. Am. Chem. Soc.* **1951**, *73*, 373–380.
(28) Baker, R. W. In *Membrane Technology and Applications*; Wiley: Chichester, New York, 2004; p 538.
(29) Zeman, L. J.; Zydney, A. L. In *Microfiltration and Ultrafiltration: Principles and Applications*; Marcel Dekker: New York, 1996; p 642.
(30) Ho, W. S. W.; Sirkar, K. K. In *Membrane Handbook*; Kluwer Academic: Boston, 2001; p 954.

AM8001428